Coupled Dynamic–Thermodynamic Forcings during Tropical Cyclogenesis. Part II: Axisymmetric Experiments

BRIAN H. TANG

Department of Atmospheric and Environmental Sciences, University at Albany, State University of New York, Albany, New York

(Manuscript received 16 February 2017, in final form 25 April 2017)

ABSTRACT

An ensemble of axisymmetric model experiments with simplified physics is used to evaluate the diagnostic framework presented in Part I. The central piece of the framework is understanding what causes decreases in the ratio of bulk differences of moist entropy over differences of angular momentum between two defined regions, the boundary between the two demarcating the approximate location of the emergence of the radius of maximum wind of the developing meso-beta-scale protovortex. Within a day before tropical cyclogenesis, the moist entropy forcing results in a decrease of this ratio. Net advective fluxes act to export moist entropy from the outer region and import moist entropy into the inner region, resulting in a positive radial gradient in gross moist stability that is maximized around the time of genesis. While surface moist entropy fluxes are needed for genesis to occur, they act synergistically with the net advective fluxes to decrease the ratio before and during genesis. Within a day after tropical cyclogenesis, surface moist entropy fluxes directly amplify the positive difference in moist entropy between the inner and outer regions, and radial fluxes of angular momentum reduce the magnitude of the negative difference in angular momentum between the inner and outer regions. Both of these processes act to reduce the ratio further. The framework highlights differences in processes occurring before, during, and after genesis as the meso-beta-scale protovortex develops and intensifies.

1. Introduction

There exist multiscale dynamical and thermodynamical components that must be considered in combination to understand tropical cyclogenesis. A few key components before and during tropical cyclogenesis are the moistening of a meso-beta-scale deep-tropospheric region in the inner region of a tropical disturbance (Bister and Emanuel 1997; Raymond et al. 1998, 2011; Davis and Ahijevych 2012; Wang 2012; Komaromi 2013; Zawislak and Zipser 2014), the increasing depth and amplitude of the warm core (Dolling and Barnes 2012; Zhang and Zhu 2012; Cecelski and Zhang 2013; Kerns and Chen 2015), and the formation of the meso-beta-scale, low-level protovortex within the larger meso-alpha-scale circulation (Nolan 2007; Dunkerton et al. 2009; Wang et al. 2010; Montgomery et al. 2012; Lussier et al. 2014; Wang 2014; Kilroy et al. 2017).

Tang (2017, hereafter Part I) introduced a coupled dynamic–thermodynamic diagnostic framework that allows for the investigation of processes responsible for the development of these components. The key metric χ is defined as the ratio of bulk differences in moist entropy Δs over bulk differences in angular momentum ΔM between an inner and outer region (Fig. 1a). The inner cylindrical region has a radius of r_i, and the outer annular region extends from r_i to r_o. Both regions have a height of z_t. The time tendency of χ is of particular relevance:

$$\frac{\partial \chi}{\partial t} = \underbrace{\frac{\alpha}{\Delta M}\frac{\partial}{\partial t}(\Delta s)}_{\sigma_s} - \underbrace{\frac{\alpha \Delta s}{(\Delta M)^2}\frac{\partial}{\partial t}(\Delta M)}_{\sigma_M}, \qquad (1)$$

where α is a nondimensionalization factor (see Part I), σ_s is the moist entropy forcing, and σ_M is the angular momentum forcing. Moistening and the amplification of the warm core within the inner region at a greater rate than the outer region results in a more positive Δs and more negative χ, because ΔM must be negative in order for the vortex to be inertially stable. Concentrating angular momentum in the inner region at a faster rate than the outer region, as the protovortex spins up and the

Corresponding author: Brian H. Tang, btang@albany.edu

DOI: 10.1175/JAS-D-17-0049.1

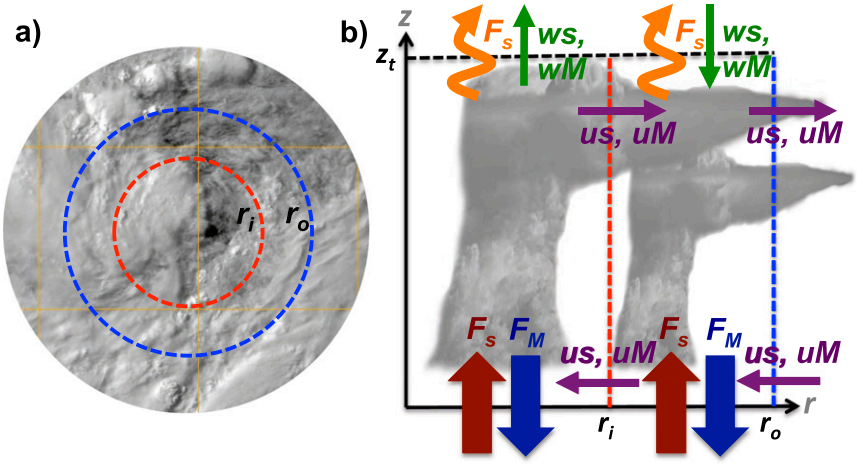

FIG. 1. (a) A planar view of a hypothetical tropical disturbance. The inner cylindrical region extends to r_i, and the outer annular region extends from r_i to r_o. Both regions extend from the surface to z_t. (b) Moist entropy and angular momentum budgets in each region. Purple arrows are radial advective fluxes through r_i and r_o, green arrows are vertical advective fluxes through z_t, orange arrows are radiative fluxes of moist entropy at z_t, red arrows are surface fluxes of moist entropy, and blue arrows are surface fluxes of angular momentum. Figure is adapted from Part I.

radius of maximum wind begins to contract inward in the inner region, resulting in a less negative ΔM and a more negative χ. It is therefore reasonable to postulate that a decrease in χ signifies tropical cyclogenesis is occurring, but what is the character of this decrease (i.e., more gradual versus abrupt)? What is the relative importance of changes in Δs and/or ΔM toward decreasing χ before, during, and after genesis?

A principle advantage of using moist entropy and angular momentum is that their budgets can be easily quantified over both the inner and outer regions (Fig. 1b), thereby allowing σ_s and σ_M to be expanded:

$$\sigma_s = \frac{\alpha}{\Delta M}\left[-\left(\frac{1}{m_i}+\frac{1}{m_o}\right)\int_0^{z_t}\int_0^{2\pi}(u-\dot r_i)\rho s r|_{r_i}\,d\theta\,dz + \frac{1}{m_o}\int_0^{z_t}\int_0^{2\pi}(u-\dot r_o)\rho s r|_{r_o}\,d\theta\,dz \right.$$
$$-\frac{1}{m_i}\int_0^{2\pi}\int_0^{r_i} w\rho s|_{z_t} r\,dr\,d\theta + \frac{1}{m_o}\int_0^{2\pi}\int_{r_i}^{r_o} w\rho s|_{z_t} r\,dr\,d\theta$$
$$\left.+\frac{1}{m_i}\int_0^{2\pi}\int_0^{r_i} F_s^{\rm net} r\,dr\,d\theta - \frac{1}{m_o}\int_0^{2\pi}\int_{r_i}^{r_o} F_s^{\rm net} r\,dr\,d\theta\right] \tag{2}$$

and

$$\sigma_M = \frac{\alpha\Delta s}{(\Delta M)^2}\left[\left(\frac{1}{m_i}+\frac{1}{m_o}\right)\int_0^{z_t}\int_0^{2\pi}(u-\dot r_i)\rho M r|_{r_i}\,d\theta\,dz - \frac{1}{m_o}\int_0^{z_t}\int_0^{2\pi}(u-\dot r_o)\rho M r|_{r_o}\,d\theta\,dz\right.$$
$$+\frac{1}{m_i}\int_0^{2\pi}\int_0^{r_i} w\rho M|_{z_t} r\,dr\,d\theta - \frac{1}{m_o}\int_0^{2\pi}\int_{r_i}^{r_o} w\rho M|_{z_t} r\,dr\,d\theta$$
$$\left.-\frac{1}{m_i}\int_0^{2\pi}\int_0^{r_i} F_M|_{z=0} r\,dr\,d\theta + \frac{1}{m_o}\int_0^{2\pi}\int_{r_i}^{r_o} F_M|_{z=0} r\,dr\,d\theta\right], \tag{3}$$

where m_i is the mass of the inner region, m_o is the mass of the outer region, u is the radial wind, w is the vertical wind, $\dot r_i$ and $\dot r_o$ are the time rates of change of r_i and r_o (see Part I), ρ is the dry density, $F_s^{\rm net}$ is the net column nonadvective flux of moist entropy, and F_M is boundary fluxes of angular momentum. See Part I for explanations of the terms. Equations (2) and (3) allow one to assess which processes are important to changing χ and when.

For example, a net advective flux of moist entropy from the outer to inner regions might yield a negative σ_s, decreasing χ. Larger surface enthalpy fluxes in the inner region compared to the outer region might also yield a negative σ_s. Likewise, one may obtain similar relationships between σ_M and its components.

Differences in the net advective flux of moist entropy in the inner and outer regions serve as a bulk metric of radial gradients of the gross moist stability (GMS), provided there is mean ascent in both the inner and outer regions. While a lower GMS has been hypothesized to favor bottom-heavy convective mass flux profiles that quickly spin up the low-level vortex (Raymond and Sessions 2007; Raymond et al. 2007, 2014), the role of radial gradients and the time evolution of the GMS around tropical cyclogenesis remain to be investigated.

We will apply the framework in a set of axisymmetric hurricane model experiments. Section 2 describes the modeling methodology. Section 3 explains how genesis is defined in the experiments. Section 4 analyzes the experiments using the framework. Section 5 ends with conclusions.

2. Methodology

a. Model

The model used in this study is the Axisymmetric Simplified Pseudoadiabatic Entropy Conserving Hurricane (ASPECH) model (Tang and Emanuel 2012, hereafter TE12), a nonhydrostatic model phrased in radius–height coordinates. The domain extends to 1500 km in radius and 25 km in height. The radial grid spacing is 2 km, and the vertical grid spacing is 0.3 km. The Coriolis parameter is fixed at $5.0 \times 10^{-5}\,\mathrm{s}^{-1}$. A simple set of parameterizations is used. Radiation is parameterized through a constant radiative cooling rate of $-2\,\mathrm{K\ day}^{-1}$ in the troposphere, which is typical for clear-sky conditions in the tropics (Hartmann et al. 2001). There are no cloud–radiative feedbacks. Microphysics is parameterized using the Kessler scheme (Kessler 1969) with a constant terminal velocity for rain of $-7\,\mathrm{m\,s}^{-1}$. Turbulence is parameterized using the methodology of Bryan and Rotunno (2009), except using the fully compressible equations. Surface fluxes are parameterized using bulk aerodynamic formulas. The enthalpy exchange coefficient is fixed at 1.2×10^{-3}, and the drag coefficient is fixed at 1.5×10^{-3}, which are approximate values at surface wind speeds between 10 and $20\,\mathrm{m\,s}^{-1}$ (Black et al. 2007). There is no convective parameterization. The purpose of using a simple set of parameterizations is to reduce the degrees of freedom in the model to test the essence of the framework.

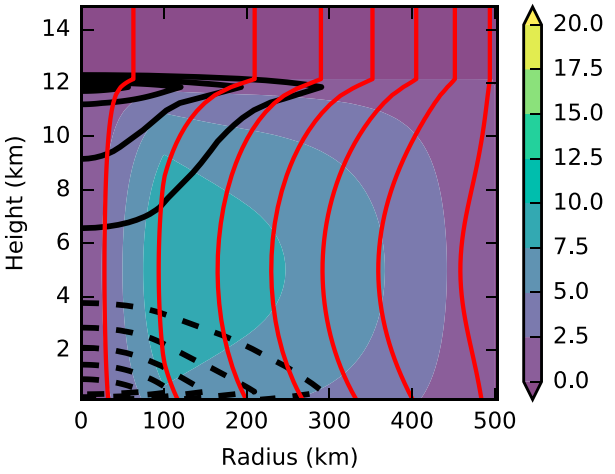

FIG. 2. Initial tangential wind (shaded; $\mathrm{m\,s}^{-1}$), horizontal moist entropy perturbations (black contours; every $2.5\,\mathrm{J\,kg}^{-1}\,\mathrm{K}^{-1}$ with negative values dashed and zero line omitted), and angular momentum (red contours; every $10^6\,\mathrm{m}^2\,\mathrm{s}^{-1}$ beginning at $0.1 \times 10^6\,\mathrm{m}^2\,\mathrm{s}^{-1}$).

ASPECH is a finite-volume model and fully conservative in the absence of boundary sources and sinks. Moist entropy and angular momentum are prognostic variables. The conservative nature of the model allows for an accurate accounting of the components of σ_s and σ_M, which would otherwise potentially have large residuals for a model that uses numerical methods that are approximately conservative or does not have a prognostic moist entropy equation. Details of the numerical methods of ASPECH are given in TE12.

b. Initial conditions

The model is initialized with a balanced vortex that has a maximum tangential wind of $10\,\mathrm{m\,s}^{-1}$ at 100-km radius and 5-km height (Fig. 2). The radial structure of the vortex is specified using (6) from Knaff et al. (2011) with a radius of zero wind of 500 km. The vertical structure is the square root of a half cosine profile, such that the vortex vanishes above 12 km. The initial maximum tangential wind at the surface is about $6\,\mathrm{m\,s}^{-1}$. Angular momentum contours bow inward where the tangential wind is positive, reaching their apex at 5-km height.

The temperature and moisture profiles are initialized with the Dunion (2011) moist tropical sounding. The temperature and moisture are adjusted to be in thermal-wind balance with the vortex, adapted from the procedure of Smith (2006), such that the relative humidity is constant with radius. Positive moist entropy perturbations exist above 5 km, while negative moist entropy perturbations exist below 5 km within 300 km.

An ensemble of 20 experiments is generated by adding uniformly distributed, random perturbations to the initial water vapor mixing ratio in the lowest three

model levels, similar to the methodology of Van Sang et al. (2008). The perturbations are randomly drawn from a uniform distribution between -1 and $+1\,\mathrm{g\,kg^{-1}}$ with a mean of zero and are different for each experiment. Small differences in the initial condition generate spread in the spinup evolution in the experiments. The spread is fundamental to the stochastic nature of convection and its upscale effects on the circulation (Zhang and Sippel 2009; Tang et al. 2016). An ensemble average filters out a portion of the stochastic component, yielding a higher signal-to-noise ratio.

3. Genesis interval

It is convenient to have some objective measure of genesis time. We define an objective genesis time in ASPECH based on three threshold conditions that must be met for all 6-h periods subsequent to the genesis time. Each threshold condition has a range, yielding a large number of possible genesis times, acknowledging that tropical cyclogenesis is a continuous, nonmonotonic process that does not lend itself well to a single univariate threshold.

The first condition is that the 6-h average 10-m maximum wind speed $v_{10\mathrm{m}}$ must exceed a value ranging from 10 to $15\,\mathrm{m\,s^{-1}}$. While there is no explicit minimum intensity required for a tropical depression (American Meteorological Society 2012), this range encompasses typical operational intensities of tropical depressions and is larger than the initial maximum wind speed at the surface. The second condition is that the standard deviation of r_{80}, the innermost radius at which the 10-m wind speed equals 80% the 10-m maximum wind speed (Nguyen et al. 2014), must be less than a value ranging from 15 to 30 km. The advantage of using r_{80} over the radius of maximum wind is that r_{80} is a more stable metric for weak, flat radial wind profiles. This condition requires there to be coherence in the vortex, associated with the formation of a compact vortex that is subsequently sustained within the broader circulation (Nolan 2007). The third condition is that the mode of z_{80}, the lowest height at which the wind equals 80% the maximum wind speed anywhere in the domain, must be less than a value ranging from 1 to 2.5 km. The vortex should have its maximum amplitude at low levels, which is a defining characteristic of a tropical cyclone.

Each range for the three conditions is divided into 10 values, yielding 1000 genesis times when considering all possible combinations. The minimum and maximum of the genesis times defines a genesis interval. The genesis interval accounts for uncertainty in the genesis time in a robust manner, but it should be noted that any criteria for genesis will be arbitrary to some degree. The mean of the genesis times for each experiment will serve as an anchor point for compositing, and we will call this mean the "genesis time" for simplicity.

Figure 3 shows Hovmöller diagrams of $v_{10\mathrm{m}}$, r_{80}, and z_{80} for a sample of experiments. Through the first day, $v_{10\mathrm{m}}$ mostly remains under $10\,\mathrm{m\,s^{-1}}$ and then varies around $10\,\mathrm{m\,s^{-1}}$ up to the start of the genesis interval. Before genesis, there is relatively large variability in r_{80} that is tied to transient features that propagate radially inward. There are also short periods where the vortex is strongest above 2.5 km, but z_{80} is predominately at or below 1 km. The lack of longer periods where the midlevel vortex is stronger than the low-level vortex is likely due to the lack of ice microphysics, which is important for stratiform precipitation and the resulting midlevel inflow that spins up the midlevel vortex (Grabowski 2003). Through the genesis interval, there is a trend toward intensification of the vortex and a consolidation of r_{80} around 100 km. After the genesis interval, the vortex continues to intensify and r_{80} generally contracts inward.

The genesis time ranges from 64 to 85 h in the ensemble of experiments (Fig. 4). The spread is representative of the stochastic effects of convection and ranges for the three conditions, representing the uncertainty in genesis times in ASPECH. The genesis interval width for each individual experiment varies from a few hours (Fig. 3a) to about a day (Fig. 3c), indicating a spectrum of abrupt to gradual developments. The mean genesis interval width is about 12 h.

Figures 5a, 5d and 5g show the composite ensemble-mean structure 0–24 h prior to the start of the genesis interval. The vortex has a broad area of winds between 10 and $12.5\,\mathrm{m\,s^{-1}}$ in the lower half of the troposphere. The angular momentum contours have moved inward in the lower troposphere compared to their initial position (Fig. 2). Furthermore, the initial negative moist entropy perturbations have decayed and switched to positive moist entropy perturbations within 300 km, reaching a maximum of greater than $25\,\mathrm{J\,kg^{-1}\,K^{-1}}$ at 4 km in height and 100 km in radius.

The moist entropy perturbations can be divided into the part due to potential temperature perturbations and the part due to moisture perturbations. Most of the positive moist entropy perturbations are due to moisture perturbations (Fig. 5g), although a weak warm core is beginning to develop (Fig. 5d) before the genesis interval.

During the genesis interval (Figs. 5b,e,h), the vortex has intensified further with a sharper radial peak in the tangential winds between 100 and 150 km, where the maximum tangential winds have increased to greater than $15\,\mathrm{m\,s^{-1}}$ around 1–2 km in height. The sharper radial peak marks the formation of a more coherent radius of maximum wind, as inferred by the decrease in

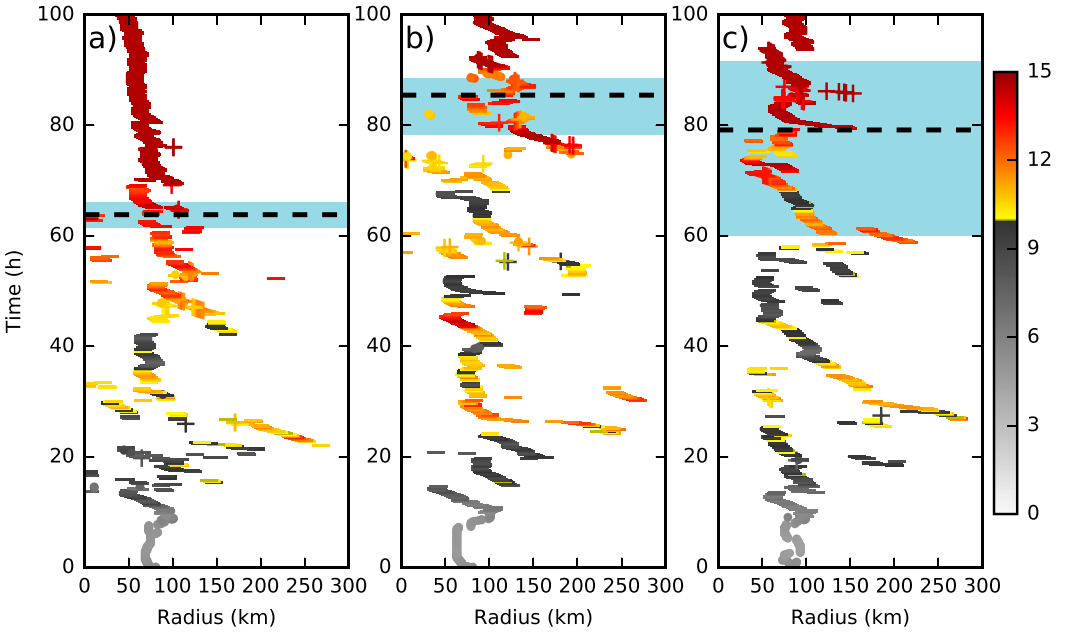

FIG. 3. Hovmöller diagrams of v_{10m}, r_{80}, and z_{80} for the experiment with (a) the earliest genesis interval, (b) the latest genesis interval, and (c) the longest genesis interval. The value of r_{80} is given along the abscissa. Dashes, dots, and plus signs indicate z_{80} is below 1.0 km, between 1.0 and 2.5 km, and above 2.5 km in height, respectively. The color shading of each symbol gives v_{10m} ($m\,s^{-1}$) according to the scale. The light blue shading is the genesis interval, and the thick dashed line is the mean genesis time.

variance in r_{80} during the genesis interval (Fig. 3). The radial angular momentum gradient in the lower troposphere also increases as angular momentum contours move inward. Additionally, the positive moist entropy perturbations have increased in magnitude to greater than $30\,J\,kg^{-1}\,K^{-1}$ as a result of continued increases in the moisture perturbations (Fig. 5h). The positive moist entropy perturbations also increase in areal extent, as the warm core strengthens inward of 150 km (Fig. 5e).

Within the 24 h after the end of the genesis interval (Fig. 5c), the vortex intensifies further, and the radius of maximum wind contracts inward. The radial gradient of angular momentum increases, particularly on the radially inward side of the radius of maximum wind. In this same region, the moist entropy perturbations continue to increase, reaching a maximum greater than $35\,J\,kg^{-1}\,K^{-1}$. The depth of the positive moist entropy perturbations also grows as a result of the amplifying warm core (Fig. 5f), consistent with the early stages of the development of the warm-core structure in 3D model simulations (Stern and Nolan 2012). The increase in the moist entropy perturbation magnitude and depth is consistent with composite dropsonde observations around genesis (Zawislak and Zipser 2014).

Figure 5 paints a complex evolution of the moist entropy and angular momentum fields. We now use the diagnostic framework to investigate the roles of the moist entropy and angular momentum forcing components around tropical cyclogenesis.

4. Framework evaluation

The framework requires specification of initial values of r_i, r_o, and z_t. As explained in Part I, r_i is chosen to

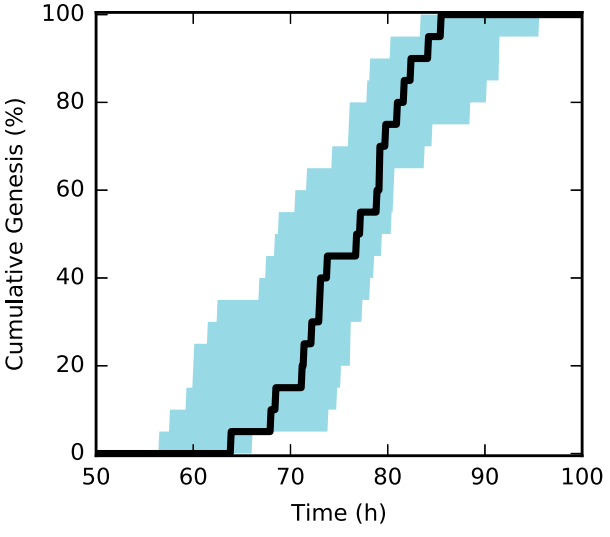

FIG. 4. Cumulative distribution of the genesis interval bounds (light blue shading) and the mean genesis time (black line) for all the experiments.

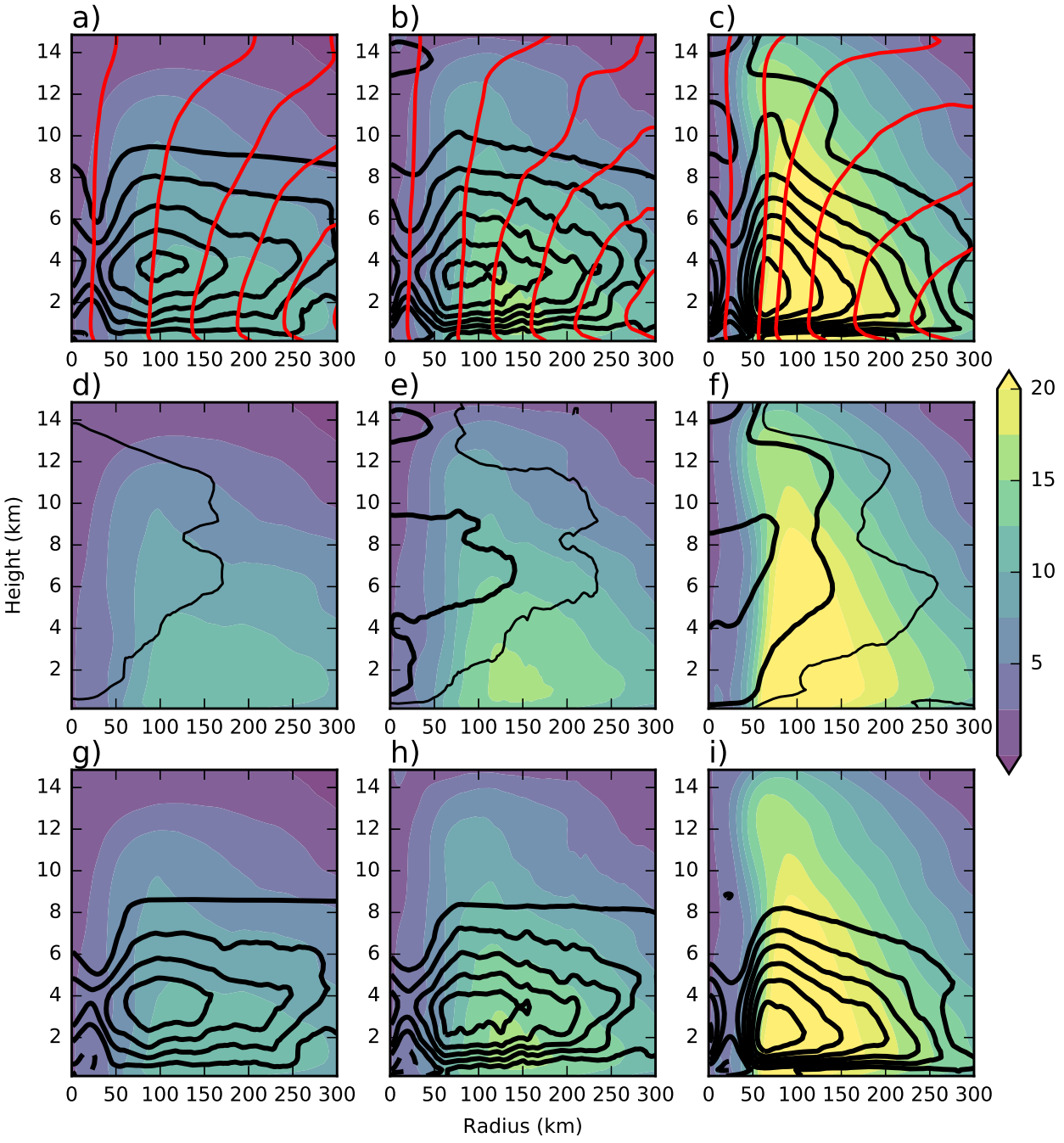

FIG. 5. (a)–(c) Composite ensemble-mean tangential wind (shaded; $m\,s^{-1}$), horizontal moist entropy perturbations (black contours; every $5\,J\,kg^{-1}\,K^{-1}$ with negative values dashed and zero line omitted), and angular momentum (red contours; every $10^6\,m^2\,s^{-1}$ beginning at $0.1 \times 10^6\,m^2\,s^{-1}$). (d)–(f) Black contours are the potential temperature component of the horizontal moist entropy perturbations (additional thin contour is $+2.5\,J\,kg^{-1}\,K^{-1}$). (g)–(i) Black contours are the moisture component of the horizontal moist entropy perturbations. Time averages are (a),(d),(g) 24-h period prior to the start of the genesis interval; (b),(e),(h) genesis interval; and (c),(f),(i) 24-h period after the end of the genesis interval.

be the approximate location where the low-level radius of maximum wind emerges in order to understand processes around the emerging meso-beta-scale protovortex. The ensemble-mean radius of maximum 10-m wind is 125 km during the genesis interval, with 80% of the experiments lying between 100 and 150 km (not shown). Note that this choice of r_i is particular to this set of ASPECH experiments and would likely

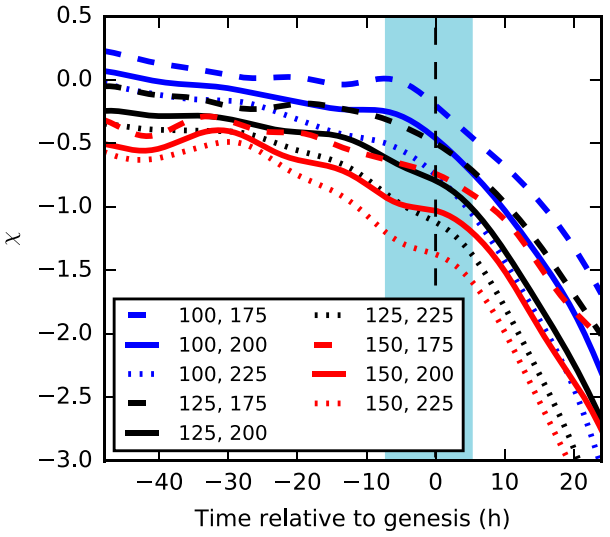

FIG. 6. Composite ensemble-mean time series of the low-pass-filtered χ for combinations of three initial r_i and three initial r_o, given in the legend (km). The light blue shaded area here and in all subsequent figures is the mean genesis interval.

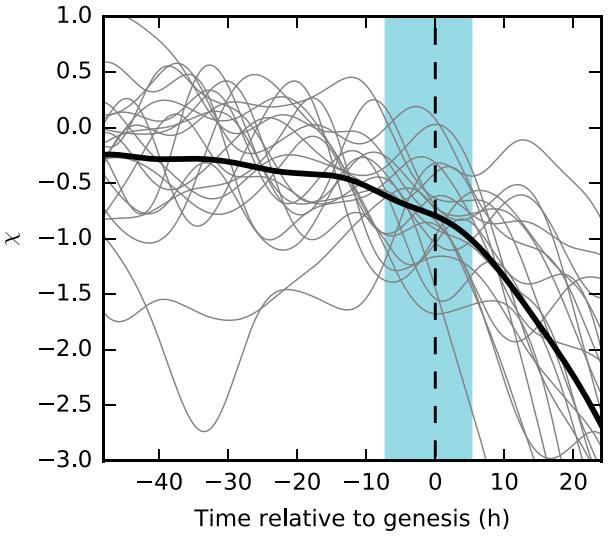

FIG. 7. As in Fig. 6, but for only an initial r_i = 125 km and r_o = 200 km. The thin, gray lines denote each experiment, and the thick black line denotes the ensemble mean.

be different for other initial conditions or model experiments.

To test how the choice of initial r_i and r_o affects the behavior of χ, we choose the initial r_i to be 100, 125, or 150 km and the initial r_o to be 175, 200, or 225 km. We fix z_t at 17 km, just above the height of the initial tropopause, such that the full secondary circulation is captured. The combinations of r_i and r_o yield nine possible domains.

For each experiment and domain, χ is calculated. A low-pass finite impulse response filter is then applied to remove high-frequency variability at periods less than half a day to filter out unbalanced "noise," since a key assumption of the framework is that the azimuthal-average vortex above the boundary layer is nearly in balance on time scales greater than half a day. The experiments are then composited relative to their individual genesis times. Unless otherwise stated, all figures hereafter show low-pass-filtered and composited variables.

Figure 6 shows the ensemble mean χ for the nine different domains. As r_i increases for fixed r_o (from blue, to black, to red lines for a fixed line style), χ decreases. As the inner region gets larger, it encompasses a greater portion of the most positive moist entropy anomalies (Fig. 5), resulting in an increase in Δs. As r_o increases for fixed r_i (from dashed, to solid, to dotted lines for a fixed color), χ also decreases. As the outer region gets larger, it encompasses a greater portion of the smaller moist entropy anomalies. As a result, Δs also increases with increasing r_o. In the limit the outer region extends to very large radius, the outer region would effectively represent the environment. Having too large of an outer or inner region would render the framework less useful, as it would lack resolution of processes occurring around the radius of maximum wind of the developing protovortex. Having too small of an outer or inner region could violate the assumption that the regions exist in a quasi-balanced state and potentially lead to increased unbalanced noise. Note that ΔM is also affected by the choice of r_i and r_o, but the nondimensionalization factor α eliminates the sensitivity (see Part I). Additionally, there is little sensitivity in χ when varying z_t from the middle troposphere to lower stratosphere (not shown).

Even though the magnitude and sign of χ are sensitive to the initial choice of r_i and r_o, there are common traits in the evolution of χ across all the domains. The curves in Fig. 6 roughly parallel each other. Before the genesis interval, χ is either flat or slowly decreasing. The magnitude of χ generally remains below 1.0, indicating that the magnitude of $\Delta s \Delta M^{-1}$ is less than or equal to α^{-1}, the chosen reference value. After the genesis interval, χ is clearly decreasing at a much faster rate than before the genesis interval. The genesis interval itself represents a transition period.

Hereafter, we only analyze the domain with an initial r_i of 125 km and r_o of 200 km. This domain has a r_i near the ensemble mean radius of maximum 10-m wind.

Figure 7 shows the evolution of χ for the individual experiments and the ensemble mean. The ensemble mean dampens the variability seen in each experiment. While there is a tendency for a slow decrease before the start of the genesis interval, most of the experiments have oscillations between −1.0 and 0.5. The oscillations in χ are inferred to be the manifestation of convective

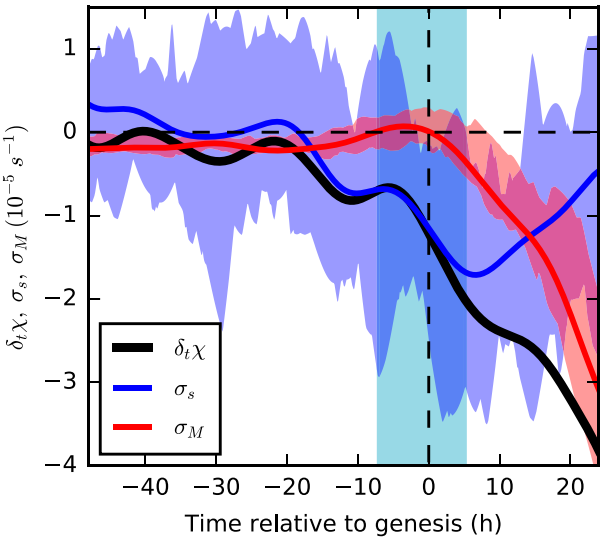

FIG. 8. Composite ensemble-mean time series of the low-pass-filtered time tendency of χ (black line), moist entropy forcing (blue line), and angular momentum forcing (red line). Shaded areas give the interquartile range of the moist entropy forcing and angular momentum forcing.

bursts modifying the moist entropy and, to a lesser extent, the angular momentum in each region. Within the genesis interval or shortly after, χ in almost all of the experiments begins to sharply decrease. The key question is what processes are responsible for the decrease in χ.

The decrease in χ is investigated by taking the time tendency of χ over a moving 6-h window and calculating σ_s and σ_M over the same window (Fig. 8). Before −20 h, the time tendency of the ensemble mean of χ is near zero. The ensemble-mean moist entropy and angular momentum forcing components are also near zero, but the moist entropy forcing shows much greater ensemble spread. After −20 h, the time tendency of χ decreases as a result of a concomitant decrease in the moist entropy forcing. Over the same period, the angular momentum forcing increases slightly but remains near zero. After the genesis time, the angular momentum forcing becomes negative and decreases sharply thereafter, surpassing the magnitude of the moist entropy forcing about 15 h after the genesis time. Meanwhile, the moist entropy forcing increases, but still generally remains negative, consistent with the expansion of the high-entropy core (Fig. 5c). Hence, in the period from −12 h to the end of the genesis interval, the decrease in χ is largely dominated by the moist entropy forcing. After the genesis interval, the moist entropy forcing and angular momentum forcing are both important, but the angular momentum forcing has an increasing role in further decreasing χ.

Figure 9 shows the components of the moist entropy forcing, the rhs of (2). The first pair of terms on the rhs of (2) represent the radial advective flux component, and the second pair of terms represent the vertical advective flux component. The largest components are the radial advective flux and the vertical advective flux (Fig. 9a). The two nearly cancel each other out, making it important to have accurate and high-time-resolution output of the advective fluxes. Figure 9a also indicates vertical fluxes of moist entropy at the domain top are large and cannot be neglected, at least in this model and these experiments. This result applies even if z_t is moved upward.

The radial and vertical advective flux components are combined to yield a total advective flux (Fig. 9b). Additionally, the surface moist entropy flux component and

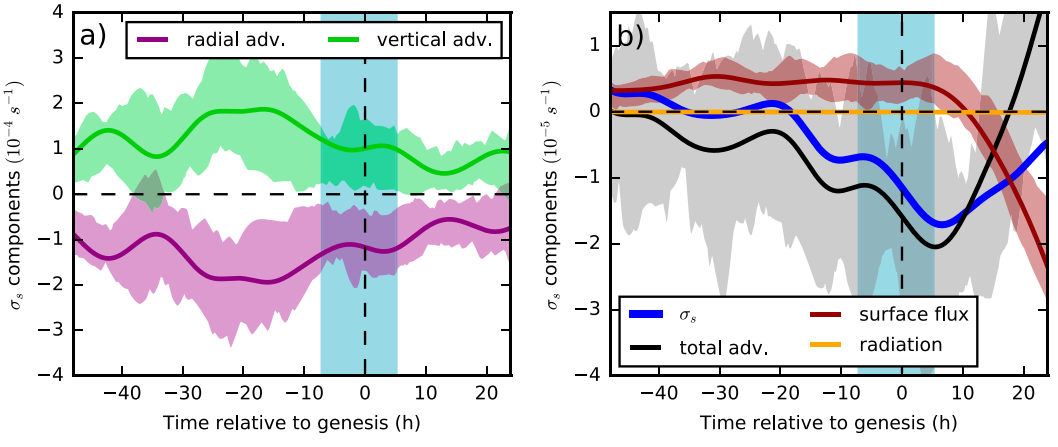

FIG. 9. Composite ensemble-mean time series of the low-pass-filtered moist entropy forcing components: (a) radial (purple) and vertical (green) advective fluxes; (b) total advective flux (black), surface moist entropy flux (maroon), radiative flux (orange), and moist entropy forcing (blue). Shaded areas give the interquartile range of each component. Note the scale difference between (a) and (b).

the radiative component, constituting the final two terms on the rhs of (2), are shown to complete the budget. The moist entropy forcing parallels the total advective flux component before and during the genesis interval. The surface flux component adds a positive offset, while the radiative component is negligible. The latter is expected since the model has constant radiative cooling and cannot produce entropy gradients via radiation. Recall that negative forcing components contribute to decreasing χ. During the genesis interval, the total advective flux is responsible for decreasing χ, while the surface fluxes do the opposite. In other words, surface fluxes are acting to increase the moist entropy in the outer region more than in the inner region. It is not until about 10 h after the genesis time that the surface flux component switches from positive to negative, and the surface flux component subsequently contributes to decreasing χ. On the other hand, the total advective flux component does the opposite, switching from negative to positive about 18 h after the genesis time.

Since the advective flux component largely controls the moist entropy forcing before and during the genesis interval, the advective flux is examined in further detail. Figure 10 shows the net advective flux tendency of the moist entropy forcing partitioned for the inner and outer regions. Positive values indicate a net import of moist entropy into a region, or a negative GMS, whereas negative values indicate a net export of moist entropy out of a region or a positive GMS. More than 40 h before the genesis time, the net advective tendencies in both regions are positive and about equal. As genesis approaches, the net advective tendencies decrease in both regions, but at a faster rate in the outer region. At −20 h, the ensemble-mean net advective tendency in the outer region becomes negative, indicating that there has been a switch from a net import to a net export of moist entropy in the outer region. Meanwhile, there is still a net import of moist entropy into the inner region. Therefore, advective fluxes cause an amplification of the bulk moist entropy difference between the inner and outer regions—that is, Δs becomes more positive. The larger the separation between the net advective tendencies between the inner and outer regions, the greater the rate that advective fluxes increase Δs and the greater the increase in GMS from the inner to outer regions. The greatest separation tends to be around and during the genesis interval, consistent with the most negative total advective flux component in Fig. 9b.

This result should not be equated to mean that surface fluxes are not important leading up to genesis, as they provide a source of moist entropy to the boundary layer that is then advected inward by the radial inflow. Genesis cannot occur without surface fluxes in ASPECH. In

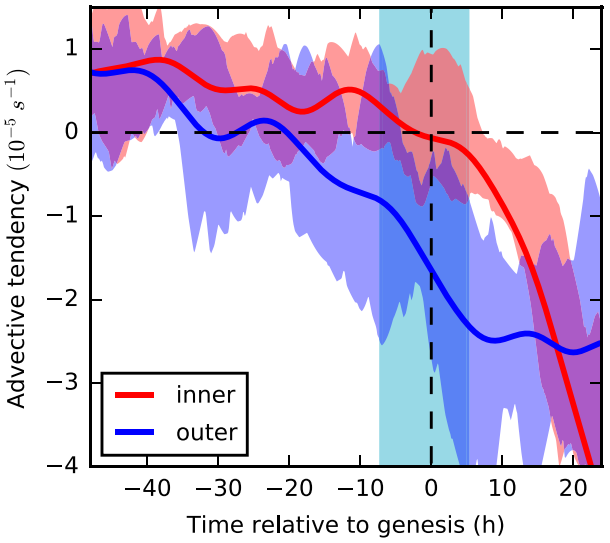

FIG. 10. Composite ensemble-mean time series of the low-pass-filtered net advective flux tendency of the moist entropy forcing in the inner (red) and outer (blue) regions. Shaded areas give the interquartile range of the tendencies in each region.

fact, increasing r_i to 250 km and r_o to 500 km results in a negative surface flux component at all times (not shown), so the surface flux component decreases χ over larger scales, a process that occurs gradually and well before tropical cyclogenesis. However, it is the synergy between surface fluxes and advection by the secondary circulation over smaller scales that results in the sharp decrease in χ in the vicinity of the emerging meso-beta-scale protovortex around the time of genesis.

After the genesis interval, the net advective flux tendency in the inner region decreases rapidly, indicating that there is also a switch from net import to net export of moist entropy in the inner region. Twenty hours after the genesis time, the net export of moist entropy in the inner region surpasses that of the outer region. However by this time, surface fluxes are acting to strongly increase Δs (Fig. 9b).

There appear to be two loose regimes controlling the moist entropy forcing and the developing high-entropy core. The first regime, during the pregenesis and genesis phases, is controlled by differences in net advective fluxes between the regions. The second regime, during the postgenesis phase, is controlled by differences in surface fluxes between the regions. The transition between the two regimes occurs quickly, in about half a day.

Figure 11 shows the components of the angular momentum forcing, the rhs of (3). Over the entire period, the radial advective flux component dominates the total budget. The ensemble-mean radial advective flux component is slightly negative prior to the genesis interval,

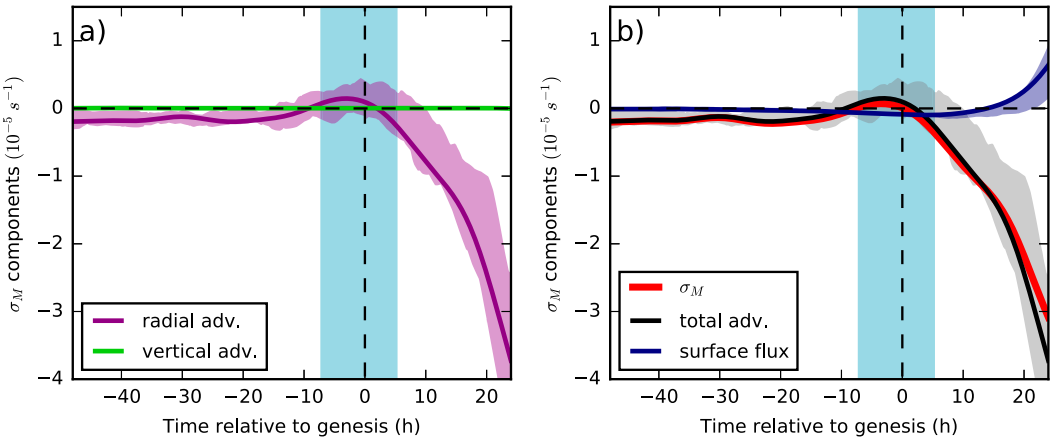

FIG. 11. As in Fig. 9, but for the angular momentum forcing components: (a) radial (purple) and vertical (green) advective fluxes; (b) total advective flux (black), surface angular momentum flux (navy), and angular momentum forcing (red).

slightly positive over the first part of the genesis interval, and then sharply decreases and becomes very negative after the genesis interval. The ensemble-mean surface flux component is negligible before the genesis interval, slightly negative during the genesis interval, and then increases and becomes positive after the genesis interval. Since the ensemble-mean Δs is positive through the period, any negative intervals in either component contribute to decreasing χ by making the magnitude of ΔM smaller.

There is a tendency for radial advective fluxes to make ΔM smaller before and after the genesis interval, but there is a curious hiatus during the first part of the genesis interval. Figure 12 shows the net advective flux tendency of the angular momentum forcing in the inner and outer regions. There is a greater positive tendency in the inner region compared to the outer region as the vortex is slowly spinning up before the genesis interval. After −15 h, the positive advective tendencies in both regions begin to increase, but the outer region does so at a slightly faster rate around the start of the genesis interval. This signature is likely tied to the formation of a coherent low-level vortex and an inward propagating radius of maximum wind that originates in the outer region before moving into the inner region (Fig. 3), but this signature is relatively weak. Bigger differences between the net advective flux tendency of the angular momentum forcing in the inner and outer regions arise after the genesis interval, as angular momentum is concentrated in the inner region by the radial inflow much more strongly compared to the outer region. Such an evolution is consistent with the tangential winds increasing strongly in the inner region, as the angular momentum contours contract inward (Fig. 5c).

Consolidating the various pieces, the negative tendency in χ prior to and during the genesis interval is due primarily to differences in net advective fluxes of moist entropy between the inner and outer regions. Thereafter, differences in net advective fluxes of angular momentum and differences in surface entropy fluxes between the two regions become important after genesis. These processes work in a coupled manner to amplify the high-entropy core and spin up the low-level vortex in the inner region, resulting in a more negative χ.

We reiterate that the results herein are particular to these set of experiments in ASPECH. Repeating the

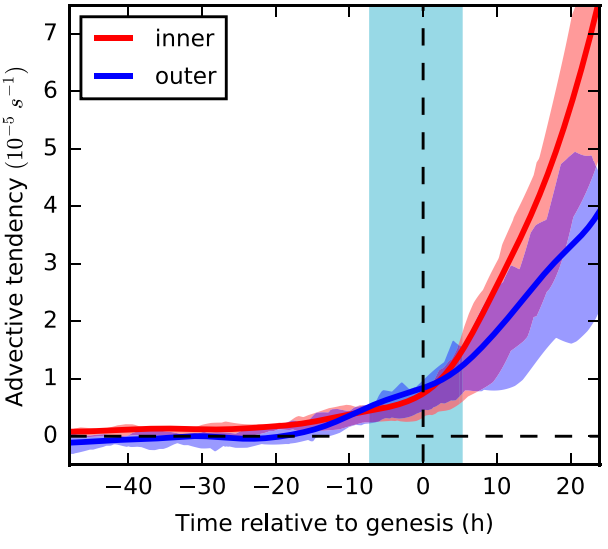

FIG. 12. As in Fig. 10, but for the net advective flux tendency of the angular momentum forcing in the inner (red) and outer (blue) regions.

framework evaluation using the different combinations of r_i and r_o shown in Fig. 6 produces qualitatively similar results, except for slightly different timings in the start of the sharp decrease of χ. For choices of $r_i > 225$ km and $r_o > 300$ km, the results differ more substantially, perhaps reflecting processes spinning up the system-scale circulation rather than the inner circulation. The spinup of the inner circulation is critical for tropical cyclogenesis, as emphasized in Nolan (2007) and Dunkerton et al. (2009), and it is important both the inner and outer regions are chosen appropriately to capture this spinup process.

5. Conclusions

An ensemble of axisymmetric tropical cyclone model experiments is used to evaluate the diagnostic framework presented in Part I. Moistening occurs well before genesis in both the inner and outer regions. Wang (2014) noted that this moistening precedes the rapid development of the tropical cyclone protovortex. Meanwhile, only a weak warm core exists prior to genesis. During genesis, continued warming and moistening of the inner region coincides with the development of a more coherent, low-level vortex. Angular momentum surfaces move inward at low levels. After genesis, frontogenesis proceeds as angular momentum and moist entropy surfaces compress in the vicinity of the radius of maximum wind, and the low-level tangential winds increase further (Emanuel 1997).

As viewed from the χ metric, χ is near zero and decreases slowly before genesis. During genesis and after, χ decreases more rapidly and becomes more negative.

The decrease in χ before and during genesis is predominately due to the moist entropy forcing and is consistent with Wang (2012). The total advective flux component dominates the moist entropy forcing, much like the horizontal fluxes of moisture dominate the water vapor budget in the inner region of a developing tropical cyclone (Fritz and Wang 2014). Net advective fluxes import moist entropy into the inner region, while net advective fluxes switch from importing to exporting moist entropy from the outer region. The net advective fluxes increase Δs and amplify the high-entropy core in the inner region. Surface fluxes, on the other hand, do not directly increase Δs before and during genesis, but surface fluxes are still important for providing a source of moist entropy to the system as a whole.

Differences in net import and export between the two regions imply there exists a positive radial gradient of GMS during tropical cyclogenesis. The traditional definition of GMS is modified to allow for moist entropy fluxes through the top of the domain, which are not generally small. The magnitude of the difference in GMS between the inner and outer regions is maximized around the genesis time. Note that this study does not prove that a positive radial gradient of GMS is necessary for tropical cyclogenesis but, rather, suggests it is a possibility. Additionally, further clarification is required to better understand the cooperative effect between radial gradients of surface fluxes and the GMS (advective fluxes).

In the day after genesis, there are substantial changes in the processes that continue to decrease χ. The surface flux component of the moist entropy forcing begins to increase Δs, as surface fluxes amplify at a greater rate in the inner region compared to the outer region. On the other hand, the total advective flux component switches from increasing to decreasing Δs. The surface flux component outpaces the total advective flux component, resulting in a net increase in Δs and a more negative χ.

The angular momentum forcing also contributes to strongly decreasing χ, surpassing the magnitude of the moist entropy forcing about 15 h after genesis. The radial flux component dominates the angular momentum forcing. The inward flux of angular momentum concentrates angular momentum more quickly in the inner region compared to the outer region. Angular momentum surfaces compress together in the inner region, accelerating frontogenesis and intensification (Emanuel 1997). As a result, the magnitude of ΔM decreases, leading to a more negative χ.

Since the advective fluxes have been shown to be important to both the moist entropy and angular momentum flux components, a logical next step would be to examine the radial structure of the vertical fluxes and the vertical structure of the radial fluxes around the time of genesis in relationship to the evolution of convective features. For example, Raymond and Sessions (2007) and Raymond et al. (2014) hypothesized that inward mass fluxes concentrated lower in the atmosphere as a result of changes in vertical stability in the presence of a midlevel vortex are important during genesis.

Limitations of the ASPECH model prevent an evaluation of some aspects of the framework. There is no ice microphysics in ASPECH, and thus no cooling due to melting and heating due to freezing. As a result, stratiform precipitation that is important to the formation of a midlevel vortex is not well represented. Inclusion of ice microphysics in the model would likely produce periods before genesis with a stronger cold anomaly in the lower troposphere and, thus, increase the variability of χ. The radial flux profiles are also different for stratiform precipitation and may change the evolution of the advective flux components. ASPECH has no radiative feedbacks that may also be important for contributing to the development of moist entropy differences between the two

regions. Radiative feedbacks have been shown to be important for the aggregation of convection in an idealized model (Wing and Emanuel 2014) and may aid tropical cyclogenesis as well (Wing et al. 2016). Another limitation is the representation of genesis with a 2D model with rings of convection versus a 3D model with more realistic convection. It would be interesting to see if the results from this study hold for an ensemble of 3D simulations and is the subject of future work. Last, it would be interesting to repeat these experiments for a mix of cases that do undergo genesis and fail to undergo genesis to determine which conditions are necessary for genesis or sufficient to prohibit genesis.

While observations are not of high-enough time and spatial resolution to fully take advantage of the framework, composites of dropsondes and/or remotely sensed variables in developing disturbances may be used to calculate bulk differences of moist entropy and angular momentum across meso-beta-scale regions separated by the emerging radius of maximum wind in order to assess whether there is a similar behavior of χ around the time of genesis. Full-physics 3D model simulations or ensembles could then be used to assess the processes controlling χ for real-world cases. A reexamination of cases from past field campaigns using this framework could be a useful starting point.

Acknowledgments. Will Komaromi and two anonymous reviewers helped improve the manuscript. The University at Albany Faculty Research Award Program Award 64949 supported a portion of this work.

REFERENCES

American Meteorological Society, 2012: Tropical depression. Glossary of Meteorology. [Available online at http://glossary.ametsoc.org/wiki/Tropical_depression.]

Bister, M., and K. A. Emanuel, 1997: The genesis of Hurricane Guillermo: TEXMEX analyses and a modeling study. *Mon. Wea. Rev.*, **125**, 2662–2682, doi:10.1175/1520-0493(1997)125<2662:TGOHGT>2.0.CO;2.

Black, P. G., and Coauthors, 2007: Air–sea exchange in hurricanes: Synthesis of observations from the Coupled Boundary Layer Air–Sea Transfer experiment. *Bull. Amer. Meteor. Soc.*, **88**, 357–374, doi:10.1175/BAMS-88-3-357.

Bryan, G. H., and R. Rotunno, 2009: The maximum intensity of tropical cyclones in axisymmetric numerical model simulations. *Mon. Wea. Rev.*, **137**, 1770–1789, doi:10.1175/2008MWR2709.1.

Cecelski, S. F., and D.-L. Zhang, 2013: Genesis of Hurricane Julia (2010) within an African easterly wave: Low-level vortices and upper-level warming. *J. Atmos. Sci.*, **70**, 3799–3817, doi:10.1175/JAS-D-13-043.1.

Davis, C. A., and D. A. Ahijevych, 2012: Mesoscale structural evolution of three tropical weather systems observed during PREDICT. *J. Atmos. Sci.*, **69**, 1284–1305, doi:10.1175/JAS-D-11-0225.1.

Dolling, K., and G. M. Barnes, 2012: Warm-core formation in Tropical Storm Humberto (2001). *Mon. Wea. Rev.*, **140**, 1177–1190, doi:10.1175/MWR-D-11-00183.1.

Dunion, J. P., 2011: Rewriting the climatology of the tropical North Atlantic and Caribbean Sea atmosphere. *J. Climate*, **24**, 893–908, doi:10.1175/2010JCLI3496.1.

Dunkerton, T. J., M. T. Montgomery, and Z. Wang, 2009: Tropical cyclogenesis in a tropical wave critical layer: Easterly waves. *Atmos. Chem. Phys.*, **9**, 5587–5646, doi:10.5194/acp-9-5587-2009.

Emanuel, K. A., 1997: Some aspects of hurricane inner-core dynamics and energetics. *J. Atmos. Sci.*, **54**, 1014–1026, doi:10.1175/1520-0469(1997)054<1014:SAOHIC>2.0.CO;2.

Fritz, C., and Z. Wang, 2014: Water vapor budget in a developing tropical cyclone and its implication for tropical cyclone formation. *J. Atmos. Sci.*, **71**, 4321–4332, doi:10.1175/JAS-D-13-0378.1.

Grabowski, W. W., 2003: Impact of ice microphysics on multiscale organization of tropical convection in two-dimensional cloud-resolving simulations. *Quart. J. Roy. Meteor. Soc.*, **129**, 67–81, doi:10.1256/qj.02.110.

Hartmann, D. L., J. R. Holton, and Q. Fu, 2001: The heat balance of the tropical tropopause, cirrus, and stratospheric dehydration. *Geophys. Res. Lett.*, **28**, 1969–1972, doi:10.1029/2000GL012833.

Kerns, B. W., and S. S. Chen, 2015: Subsidence warming as an underappreciated ingredient in tropical cyclogenesis. Part I: Aircraft observations. *J. Atmos. Sci.*, **72**, 4237–4260, doi:10.1175/JAS-D-14-0366.1.

Kessler, E., 1969: *On the Distribution and Continuity of Water Substance in Atmospheric Circulations. Meteor. Monogr.*, No. 32, Amer. Meteor. Soc., 88 pp.

Kilroy, G., R. K. Smith, and M. T. Montgomery, 2017: A unified view of tropical cyclogenesis and intensification. *Quart. J. Roy. Meteor. Soc.*, **143**, 450–462, doi:10.1002/qj.2934.

Knaff, J. A., C. R. Sampson, P. J. Fitzpatrick, Y. Jin, and C. M. Hill, 2011: Simple diagnosis of tropical cyclone structure via pressure gradients. *Wea. Forecasting*, **26**, 1020–1031, doi:10.1175/WAF-D-11-00013.1.

Komaromi, W. A., 2013: An investigation of composite dropsonde profiles for developing and nondeveloping tropical waves during the 2010 PREDICT field campaign. *J. Atmos. Sci.*, **70**, 542–558, doi:10.1175/JAS-D-12-052.1.

Lussier, L. L., III, M. T. Montgomery, and M. M. Bell, 2014: The genesis of Typhoon Nuri as observed during the Tropical Cyclone Structure 2008 (TCS-08) field experiment—Part 3: Dynamics of low-level spin-up during the genesis. *Atmos. Chem. Phys.*, **14**, 8795–8812, doi:10.5194/acp-14-8795-2014.

Montgomery, M. T., and Coauthors, 2012: The Pre-Depression Investigation of Cloud-Systems in the Tropics (PREDICT) experiment: Scientific basis, new analysis tools, and some first results. *Bull. Amer. Meteor. Soc.*, **93**, 153–172, doi:10.1175/BAMS-D-11-00046.1.

Nguyen, L. T., J. Molinari, and D. Thomas, 2014: Evaluation of tropical cyclone center identification methods in numerical models. *Mon. Wea. Rev.*, **142**, 4326–4339, doi:10.1175/MWR-D-14-00044.1.

Nolan, D. S., 2007: What is the trigger for tropical cyclogenesis? *Aust. Meteor. Mag.*, **56**, 241–266.

Raymond, D. J., and S. L. Sessions, 2007: Evolution of convection during tropical cyclogenesis. *Geophys. Res. Lett.*, **34**, L06811, doi:10.1029/2006GL028607.

——, C. López-Carrillo, and L. L. Cavazos, 1998: Case-studies of developing east Pacific easterly waves. *Quart. J. Roy. Meteor. Soc.*, **124**, 2005–2034, doi:10.1002/qj.49712455011.

——, S. L. Sessions, and Ž. Fuchs, 2007: A theory for the spinup of tropical depressions. *Quart. J. Roy. Meteor. Soc.*, **133**, 1743–1754, doi:10.1002/qj.125.

——, ——, and C. López-Carrillo, 2011: Thermodynamics of tropical cyclogenesis in the northwest Pacific. *J. Geophys. Res.*, **116**, D18101, doi:10.1029/2011JD015624.

——, S. Gjorgjievska, S. L. Sessions, and Ž. Fuchs, 2014: Tropical cyclogenesis and mid-level vorticity. *Aust. Meteor. Oceanogr. J.*, **64**, 11–25, doi:10.22499/2.6401.003.

Smith, R. K., 2006: Accurate determination of a balanced axisymmetric vortex in a compressible atmosphere. *Tellus*, **58A**, 98–103, doi:10.1111/j.1600-0870.2006.00149.x.

Stern, D. P., and D. S. Nolan, 2012: On the height of the warm core in tropical cyclones. *J. Atmos. Sci.*, **69**, 1657–1680, doi:10.1175/JAS-D-11-010.1.

Tang, B. H., 2017: Coupled dynamic–thermodynamic forcings during tropical cyclogenesis. Part I: Diagnostic framework. *J. Atmos. Sci.*, **74**, 2269–2278, doi:10.1175/JAS-D-17-0048.1.

——, and K. Emanuel, 2012: Sensitivity of tropical cyclone intensity to ventilation in an axisymmetric model. *J. Atmos. Sci.*, **69**, 2394–2413, doi:10.1175/JAS-D-11-0232.1.

——, R. Rios-Berrios, J. J. Alland, J. D. Berman, and K. L. Corbosiero, 2016: Sensitivity of axisymmetric tropical cyclone spinup time to dry air aloft. *J. Atmos. Sci.*, **73**, 4269–4287, doi:10.1175/JAS-D-16-0068.1.

Van Sang, N., R. K. Smith, and M. T. Montgomery, 2008: Tropical-cyclone intensification and predictability in three dimensions. *Quart. J. Roy. Meteor. Soc.*, **134**, 563–582, doi:10.1002/qj.235.

Wang, Z., 2012: Thermodynamic aspects of tropical cyclone formation. *J. Atmos. Sci.*, **69**, 2433–2451, doi:10.1175/JAS-D-11-0298.1.

——, 2014: Role of cumulus congestus in tropical cyclone formation in a high-resolution numerical model simulation. *J. Atmos. Sci.*, **71**, 1681–1700, doi:10.1175/JAS-D-13-0257.1.

——, M. T. Montgomery, and T. J. Dunkerton, 2010: Genesis of pre–Hurricane Felix (2007). Part I: The role of the easterly wave critical layer. *J. Atmos. Sci.*, **67**, 1711–1729, doi:10.1175/2009JAS3420.1.

Wing, A. A., and K. A. Emanuel, 2014: Physical mechanisms controlling self-aggregation of convection in idealized numerical modeling simulations. *J. Adv. Model. Earth Syst.*, **6**, 59–74, doi:10.1002/2013MS000269.

——, S. J. Camargo, and A. H. Sobel, 2016: Role of radiative–convective feedbacks in spontaneous tropical cyclogenesis in idealized numerical simulations. *J. Atmos. Sci.*, **73**, 2633–2642, doi:10.1175/JAS-D-15-0380.1.

Zawislak, J., and E. J. Zipser, 2014: Analysis of the thermodynamic properties of developing and nondeveloping tropical disturbances using a comprehensive dropsonde dataset. *Mon. Wea. Rev.*, **142**, 1250–1264, doi:10.1175/MWR-D-13-00253.1.

Zhang, D.-L., and L. Zhu, 2012: Roles of upper-level processes in tropical cyclogenesis. *Geophys. Res. Lett.*, **39**, L17804, doi:10.1029/2012GL053140.

Zhang, F., and J. A. Sippel, 2009: Effects of moist convection on hurricane predictability. *J. Atmos. Sci.*, **66**, 1944–1961, doi:10.1175/2009JAS2824.1.